Large-angle scattering in positron-helium and positron-krypton collisions

D. R. Schultz, C. O. Reinhold, and R. E. Olson
Department of Physics and Laboratory for Atomic and Molecular Research, University of Missouri–Rolla, Rolla, Missouri 65401
(Received 7 June 1989)

We have calculated differential cross sections as a function of the projectile scattering angle for positron-helium and positron-krypton collisions using the classical-trajectory Monte Carlo technique. These intermediate-velocity collisions have been simulated by various independent-electron and n-electron models, using both screened Coulomb and quantum model potentials to approximate the effects of electron-electron interactions. These several models all indicate that scattering of positrons to large angles in ionizing collisions persists to high impact velocities. In a previous work [Phys. Rev. A **38**, 1866 (1988)] we proposed that the recent experiments that have measured the total cross section for positronium formation could be affected by the loss of positron flux due to incomplete confinement after large-angle scattering. Here, utilizing these newly calculated differential-scattering cross sections, adjustments are computed that account for the difference between the experimental and theoretical behaviors of the positronium formation cross section. Further, it is demonstrated that large-angle scattering in the elastic channel is important for one of the experiments. We have also computed total cross sections for ionization and charge transfer for collisions of protons with krypton. Good agreement is obtained in these cases with experimental measurements.

I. INTRODUCTION

Recently there has been much interest, both experimentally and theoretically, in matter-, antimatter-atom collisions (see Refs. 1–4 and references therein). The goal of these studies has primarily been to explore effects due to the change of projectile mass and sign of charge. By considering the family of singly charged particles, electrons, positrons, protons, and antiprotons, one may vary a single-collision parameter at a time, separating out the mass and sign of the charge effects. Investigation of these processes theoretically requires treatments that go beyond simple first-order theories that often mask these effects. As well, experimental investigations of these effects have marked pioneering work in the harnessing of antimatter projectiles for use in inelastic ion-atom collisions.

The measurement of the total cross section for the formation of positronium in positron-atom collisions has provided an important point of comparison between theory and experiment relevant to these matter-, antimatter-atom studies. Fornari *et al.*,[5] Diana *et al.*,[6] and Fromme *et al.*[7] have recently undertaken this task for positron-helium collisions at intermediate velocities. However, there exists a fundamental disagreement between theory and these experiments as to the high-velocity behavior of the cross section. In a previous work, Schultz and Olson[3] proposed a resolution of this disagreement based on the hypothesis that a certain portion of positrons scattered at large angles might have been unaccounted for in the experiments.

Here, we consider in detail our previous proposal to resolve this discrepancy, performing more comprehensive calculations of the ionization differential cross section as a function of the scattering angle in positron-helium collisions, and by relating these results to the quantities measured in each of the experiments. We extend this argument to consider other scattering channels which we believe might also contribute to the discrepancies. We conclude that the experimental measurements overestimate the positronium formation cross section due to their partial sampling of other scattering channels, both elastic and inelastic. This effect is quite significant at relatively high impact velocities since the ionization and elastic cross sections are quite large as compared to that for charge transfer. Thus, sampling even a small fraction of these processes swamps the positronium formation cross section which should have, according to theoretical calculations, a very rapid decline with increasing collision velocity.

The primary aim of our previous work was to elucidate the collision dynamics responsible for the enhancement of the cross section for charge transfer in positron-helium collisions relative to that for proton-helium collisions. To see if this enhancement is also present for positron collisions with many-electron targets, and to study a system that has recently been investigated experimentally,[8] we also consider here positron- and proton-krypton collisions. We find that, indeed, at large velocities positrons are more likely to remove an electron from krypton than are equivelocity protons. However, we find that the enhancement is not as great as in helium in the velocity regime considered and that due to subshell effects the increase may not be monotonic. Unfortunately, we discover that there is again a discrepancy between theory and experiment. As in the case of positron-helium collisions, we demonstrate that this discrepancy is due to the lack of confinement in the experiment of some positrons scattered to large angles.

To treat the positron-krypton many-electron system,

we have implemented several different models that differ in the level of approximation in which the electrons are explicitly included in the calculation. Also, to verify our previous calculation of the differential scattering cross section for positron-helium collisions, we have utilized a more realistic model potential to describe the positron–target-core and active-electron–target-core interactions. These treatments are described in Sec. II. In Sec. III we present the results of our calculations of the differential scattering cross section for ionizing collisions of positrons with helium and our proposed adjustment of the experimental data. Adjunct to this we include an Appendix which details our estimation of the experimental confinement angles.

Similarly, in Sec. IV we then present ionization differential cross sections for the scattering of positrons from krypton and our proposed adjustment for the corresponding experimental measurements of the total cross section for positronium formation. In this section we also include our calculation of the total cross section for ionization and capture by protons so as to compare it with other existing experimental measurements. Thus, these proton collisions calculations serve as a benchmark for our positron calculations, as in the case of our treatment of helium. Our conclusions, concerning both systems, positron-helium and positron-krypton, are then summarized in Sec. V.

Atomic units are assumed and used throughout as are laboratory scattering angles.

II. THEORETICAL METHOD

For this study, we have utilized the classical trajectory Monte Carlo (CTMC) technique, which has been described fully by Abrines and Percival,[9] Olson and Salop,[10] and others. Briefly, the CTMC technique is a method in which a large ensemble of projectile-target configurations is sampled in order to simulate the ion-atom collision. It has been demonstrated to yield good results for ionization and charge-transfer processes in the intermediate collision velocity regime,[3,9–13] a regime in which perturbative approaches have not had as much success. The basis of its ability to accurately model such collisions rests on the fact that the projectile–active-electron and active-electron–target-core interactions are exactly taken into account.

Our previous calculation[3] of the differential cross section as a function of the scattering angle of the positron in collisions with helium indicated that significant scattering to large angles persisted to high impact velocities. These independent-electron model calculations were performed using a screened Coulomb potential to represent the active-electron–target-core and projectile-target-core interactions. In this work we test the large-angle scattering conclusion by utilizing a more detailed potential. Furthermore, in considering positron-krypton collisions, we expect that approximating these interactions by a screened Coulomb potential would not be sufficient and we have, therefore, used a model potential for this system.

Additionally, we previously demonstrated that the positron, owing to its small mass, is easily deflected by the target atom. Therefore, we have also implemented CTMC calculations which explicitly include more than one active electron to investigate the possibility of multiple scattering. This allows us to test the validity of our model potential results for the calculation of the differential cross section. Also, since krypton is a much more complex target than helium, we expect that subshell effects, especially important in the capture channel, should not be neglected at high impact velocities. For this reason, we have also performed calculations including all the shells of krypton.

The model potential that we employ for both the projectile–target-core and electron–target-core interactions has been developed by Garvey, Jackman, and Green[14] and is given by

$$V(r)=\frac{1}{r}\{(N-1)[1-\Omega(r)]-Z\}\ , \tag{1}$$

where

$$\Omega(r)=[(\eta/\zeta)(e^{\zeta r}-1)+1]^{-1} \tag{2}$$

and where $(N-1)$ is the total number of electrons in the target atomic or ionic core of nuclear charge Z. The parameters η and ζ have been found by these authors by a process of energy minimization in a modified Thomas-Fermi statistical model for all atoms and positive ions with $2\le Z\le 54$. (For example, for He they find that $\eta=2.625$ and $\zeta=1.770$.) As may be easily deduced from (1), the model potential has the correct behavior at both small and large r. That is

$$V(r)\underset{r\to 0}{\longrightarrow}-\frac{Z}{r} \tag{3}$$

and

$$V(r)\underset{r\to\infty}{\longrightarrow}-\frac{[Z-(N-1)]}{r}\ . \tag{4}$$

We test here whether or not the use of this potential, rather than the screened Coulomb potential, will affect the shape of the differential scattering cross sections. For example, for positrons which penetrate to very small values of r, the model potential presents the full nuclear charge which could enhance the backward scattering. Also, since the model potential has the correct asymptotic value, the possibility that the wrong residual charge of the target core presented by the screened Coulomb potential might influence the scattering angle would be removed. Furthermore, we expect that for positron-krypton collisions, where the potential changes rapidly within the radius of the atom from an almost fully screened value at its outer extent, to the full nuclear interaction, $36/r$ at very small-r values, such a potential would be the only reasonable method by which to treat the scattering in a one active-electron formalism.

In order to simplify our references to these various models we include in Table I a summary of the nomenclature adopted in this work. Our use of the notation "CTMC" comes from that used to describe the original three-body, screened Coulomb formulation of Abrines and Percival.[9] An extension of this method to more than

TABLE I. Nomenclature and brief characterization of the various models used in this work. The subsequent columns indicate (i) the number of active electrons, (ii) the number of target shells considered, (iii) form of the projectile–target-core, active-electron–target-core potential, and (iv) type of binding energy used. The total number of electrons considered is given by n.

Method	Number of active electrons	Number of shells	Interaction potential	Binding energy used
CTMCn	1	1 to all	Screened Coulomb	Hartree-Fock by subshells (Ref. 15)
CTMCMn	1	1 to all	Model potential	Hartree-Fock by subshells
nCTMC	n	1 to all	Screened Coulomb	Sequential (Ref. 16) ionization potential
nCTMCM	n	1 to all	Model potential	Hartree-Fock by subshells

three bodies has been made by Olson[17,18] and has been termed "nCTMC." In this work we introduce the notation "CTMCn" to denote a method in which we include n electrons through the independent-electron approximation rather than explicitly including them as in the nCTMC. The most significant difference between these models is that whereas the projectile is scattered by the n active electrons during the collision in the nCTCM, it is only scattered by one electron at a time in the CTMCn method.

If instead of the screened Coulomb potential a model potential is used, we refer to the calculations as "CTMCMn" or "nCTMCM." In addition, these models employ binding energies which are assigned according to the Hartree-Fock approximation[15] and the same interaction potential for all electrons. In contrast, the nCTMC makes use of the sequential ionization potentials derived from experiment and, consequently, the screened Coulomb potential experienced by each electron is different. In summary, the notation used here is consistent with that which has been used previously, the additional characters being intended to clarify (i) the number of electrons explicitly included or treated using the independent-electron model and (ii) which type of interaction potential is employed.

The classical trajectory Monte Carlo method, in any of the forms described above, consists of three steps: (1) initialization of the projectile-target configuration, (2) calculation of the classical trajectories, and (3) a final-state test for reaction. In the first step the active electron is randomly initialized in its orbit according to a microcanonical distribution.[9] That is, its position and momentum are specified so that on average they mimic the quantum-mechanical position and momentum distributions. In order to sample initial conditions from a microcanonical distribution, we have used the method developed in a previous work[19] which is valid for general interactions. Also, to simulate a beam of uniform cross-sectional area, the impact parameter is randomly selected so that its square is uniformly distributed between zero and some maximum impact parameter $b_{\max}$. The maximum impact parameter is chosen such that beyond this value the probability of the reaction under consideration is negligible.

In the second step, $6\mathcal{N}$ coupled ordinary differential equations, representing the Hamilton equations of motion for the $\mathcal{N}$ bodies in the collision, are integrated numerically from some large initial projectile-target separation, through the collision, and continuing to some large final separation. After integration, the relative energies between the particles is found and what reaction, if any, has occurred. Steps (1), (2), and (3) are then repeated until the statistical error of the cross section for each channel is sufficiently small.

Within the CTMCn or CTMCMn models, the cross sections may be computed in two different ways. The first method is to integrate the equations of motion for all the independent electrons for a fixed impact parameter and obtain the cross sections from the number of counts in a particular channel. The second is to calculate the multielectron transition probabilities by means of the independent-electron approximation.[20,21] For helium this procedure is straightforward since the electrons are within the same shell. For krypton, the process is more complicated since the probabilities for each subshell must be independently computed and combined. Therefore, we have used the first technique when dealing with electron removal from all the shells of krypton, as described below. When scattering from only the outer subshell of krypton or from helium is considered, we have used the second method, which we describe below. We note for clarity that the two methods yield equivalent results.

The one-electron transition probability for some channel α is

$$\tilde{P}_\alpha(b)=\frac{N_\alpha(b)}{N(b)}\ , \tag{5}$$

where $N_\alpha(b)$ is the number of successful final-state tests for channel α and $N(b)$ is the total number of events in all channels. The multielectron probabilities are then found in terms of these one-electron probabilities using the independent-electron approximation. That is, the probability of capturing m electrons, ionizing n electrons, and therefore leaving N-m-n in the target originally containing N electrons is

$$P_{mn}(b)=\sum_{m_\nu,n_\nu}\prod_\nu \begin{bmatrix} N_\nu \\ N_\nu-m_\nu \end{bmatrix}\begin{bmatrix} N_\nu-m_\nu \\ N_\nu-m_\nu-n_\nu \end{bmatrix} \times \tilde{P}_{c\nu}^{\,m_\nu}(b)\tilde{P}_{i\nu}^{\,n_\nu}(b) \times[1-\tilde{P}_{c\nu}(b)-\tilde{P}_{i\nu}(b)]^{N_\nu-m_\nu-n_\nu}, \quad (6)$$

where N_ν is the number of electrons in the subshell whose quantum numbers are collectively represented by ν; m_ν and n_ν are the numbers of electrons captured and ionized from that subshell; and $\tilde{P}_{c\nu}(b)$ and $\tilde{P}_{i\nu}(b)$ are the one-electron probabilities for charge transfer and ionization, respectively. We note that $\sum_\nu N_\nu=N$, $\sum_\nu m_\nu=m$, and $\sum_\nu n_\nu=n$. The total cross section, in the impact-parameter formulation, is then

$$\sigma_{mn}=2\pi\int_0^{b_{\max}} P_{mn}(b)b\,db \ . \quad (7)$$

When the number of counts in a channel is obtained directly, the total cross section for a particular final channel α is simply

$$\sigma_\alpha=\pi b_{\max}^2\frac{N_\alpha}{N_{\rm MC}} \ , \quad (8)$$

where N_α denotes the total number of counts in a particular channel α and $N_{\rm MC}$ is the total number of Monte Carlo trajectories.

Of course, in a many-electron target, quite a large number of processes involving the capture of m electrons, n-fold ionization, and excitation of the remaining N-m-n electrons are possible with corresponding cross sections for each process. However, in this study only relatively few processes are considered. They are (i) single ionization $\sigma_{\rm si}$, (ii) total ionization σ_i, (iii) free-electron production σ_-, and (iv) single-electron transfer σ_{10}. While the definition of single ionization is straightforward and generally recognized, we define here the cross section for the other processes so as to avoid confusion. In terms of the cross sections for m-fold charge transfer and n-fold ionization σ_{mn}, these cross sections are

$$\sigma_i=\sum_{n=1}^{N}\sigma_{0n} \ , \quad (9)$$

$$\sigma_-=\sum_{n=1}^{N}\sum_{m=0}^{N-n} n\sigma_{mn} \ , \quad (10)$$

$$\sigma_{10}=\sum_{n=0}^{N-1}\sigma_{1n} \ . \quad (11)$$

Also, we will be interested in the differential cross section in ionizing collisions and since the final positions and momenta are known, simply trigonometry yields and scattering angle θ and the differential cross section is

$$\frac{d\sigma_i}{d\Omega}(\theta)=\pi b_{\max}^2\frac{\sum_n\sum_k[P_{0n}(b_k)/\tilde{P}_i(b_k)]}{N_{\rm MC}2\pi\sin\theta\Delta\theta} \ , \quad (12)$$

where $\Delta\Omega=2\pi\sin\theta\,\Delta\theta$ and the summation over k extends over all projectiles scattered into the angular range $(\theta-\Delta\theta/2,\ \theta+\Delta\theta/2)$ having an impact parameter b_k. Similarly, when the counts in a particular channel are obtained directly we have

$$\frac{d\sigma_i}{d\Omega}(\theta)=\pi b_{\max}^2\frac{N_i(\theta)}{N_{\rm MC}2\pi\sin\theta\,\Delta\theta} \ , \quad (13)$$

where $N_i(\theta)$ is the number of counts in the ionization channel when the projectile is scattered into the angular range $(\theta-\Delta\theta/2,\ \theta+\Delta\theta/2)$.

As we have pointed out previously,[3] since within the CTMC formalism capture to any of the infinity of classically allowed states of the projectiles is possible, no threshold for the capture channel exists. Therefore, the cross section near the actual capture threshold must be corrected by approximating the proper density of final states. This is accomplished by multiplying the charge-transfer cross sections by the ratio of the mean final projectile momentum to the initial projectile momentum k_f/k_i. We note that for heavy particles (e.g., muons, protons, ions), the ratio k_f/k_i is unity except at extremely small impact velocities. We note that, since the classical model correctly describes the density of final states for the ionization (i.e., the continuum), no correction is necessary for this channel. Thus, this factor is appropriate only for charge-transfer collisions involving light particles, that is, for positron-atom collisions.

The factor k_f/k_i for positrons is given by

$$\left[\frac{k_{f\nu}}{k_i}\right]_{\bar{e}}=\left[\frac{(E-\varepsilon_\nu)}{E}\right]^{1/2} \ , \quad (14)$$

where

$$\varepsilon_\nu=E_\nu-E_{\rm Ps} \ , \quad (15)$$

and where E is the impact energy, E_ν is the binding energy of a target electron in the subshell whose quantum numbers are collectively represented by the index ν, and $E_{\rm Ps}$ is the binding energy of the ground state of positronium. The subscript $\bar{e}$ in Eq. (14) emphasizes that k_i and k_f are the initial and final momenta for the positron. From expression (14) we clearly see that k_f/k_i rapidly approaches the value one for incident energies greater than ε_ν. For example, for capture by a positron from helium, the factor k_f/k_i differs significantly from one only for impact velocities less than about 2 a.u. Similarly, for capture from the outer subshell of krypton, it is essentially one for impact velocities greater than about 1.2 a.u.

Therefore, taking into account these corrections to the calculated charge-transfer cross sections, the single-electron transfer cross section is, summed over subshells,

$$\sigma_{10}=\sum_\nu\left[\frac{k_{f\nu}}{k_i}\right]_{\bar{e}}\sigma_{10}^\nu \ , \quad (16)$$

where σ_{10}^ν is the cross section for the capture of one electron from the subshell with quantum numbers specified by the index ν. Corrections to the cross sections for total ionization and free-electron production are negligible.

We would like to note that the factor k_f/k_i was incorrectly placed in the expression for the capture probability in our previous article[3] instead of in the expression for the cross sections.

Thus, we attempt to treat as fully as possible within the classical-trajectory Monte Carlo formalism all the effects which could modify our conclusions about the nature of the wide-angle scattering of positrons in collisions with helium and krypton. That is, we include in our study treatments which (i) more accurately reproduce the potential experienced by both the projectile and target electrons, (ii) simulate the subshell structure of krypton, and (iii) possess explicit consideration of many active electrons.

III. RESULTS FOR HELIUM

Motivated by our previous observation that in positron-helium collisions the positron may be deflected to very large angles, even at high impact velocities, we have attempted to verify this result using CTMCn, CTMCMn, and nCTMCM models. To this end we have calculated differential cross sections for positron impact velocities from 2 to 4.5 a.u., the velocity range in which the theoretically calculated total cross sections for positronium formation differ largely from the experimental measurements. With these new calculations we also attempt to substantiate our hypothesis that the persistence to large impact velocities of wide-angle scattering critically affects the measured cross sections for capture by positrons and is responsible for the disagreement between theory and experiment.

In Fig. 1 we display the results of our new CTMCn, CTMCMn, and nCTMCM model calculations of the differential cross section as a function of the scattering angle of the positron in ionizing collisions. As inspection of this figure indicates, unlike the scattering of protons by helium which is extremely forwardly peaked,[3] significant positron scattering exists to even backward angles. Further, we note the agreement between our screened Coulomb, model potential, and two electron treatments. This indicates that, at least for helium targets, the screened Coulomb interaction coupled with an independent-electron approximation is sufficient to treat the scattering of positrons at intermediate velocities within our CTMC formalism. Thus, these results indicate that the wide-angle scattering of positrons is not sensitively dependent on the precise small- and large-r behavior of the potential or multiple scattering by the two target electrons.

To quantify more specifically what we mean by the fact that the wide-angle scattering is "significant," we note that for a collision velocity of 3.83 a.u. the ionization differential cross section integrated between 90° and 180° is about 10% of the total cross section. Similarly at a velocity of 4.47 a.u. the integrated differential cross section is about 6% of the total. These percentages, while not being negligible, are hardly the dominant contribution to the total ionization cross section. However, when compared with the charge-transfer cross sections, they are indeed quite large. For example, at $v=3.83$ a.u., the integrated ionization differential cross section between 90° and 180° is approximately twice as large as the total cross section for charge transfer that we find. And at a velocity of 4.47 a.u. the ionization differential cross section integrated between these angles is three times larger than the total cross section for positronium formation. Thus, in relation to the capture cross sections, the ionization cross sections at large angles is indeed very significant.

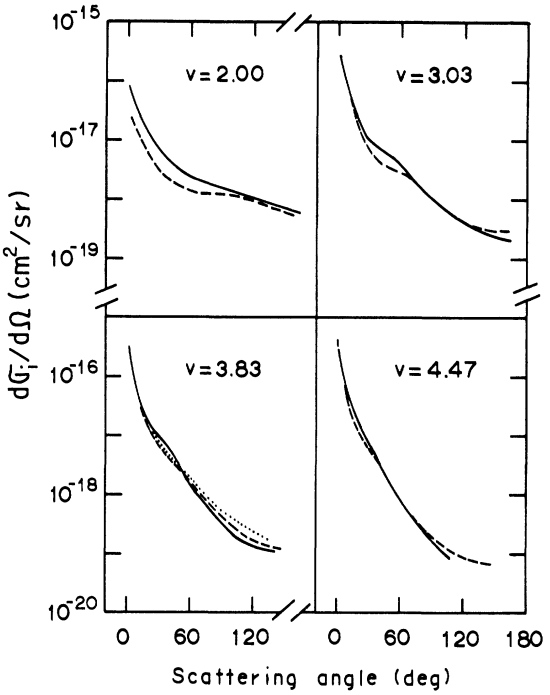

FIG. 1. The differential cross section as a function of the projectile scattering angle for ionization in collisions of positrons with helium at several velocities as indicated: CTMC2 (solid curve), CTMCM2 (dashed curves), and 2CTMCM (dotted curve).

As we have shown[3] there is a general agreement among theories that the rate of decline of the positronium formation total cross section as a function of the impact energy vary as E^{-a} where $3<a<5$, whereas the experiments by Fromme *et al.*[7] and Diana and co-workers[5,6] indicate a dependence of $1<a<1.5$. In each of the experiments, a beam of positrons is passed through a target gas region contained in a cylindrical chamber. The positrons which form positronium are removed from the beam. However, it is essential that those positrons suffering ionizing, exciting, or elastic collisions are confined to the beam in order to obtain the desired cross sections. To assure that this confinement is obtained, both experiments utilize a high axial magnetic guiding field. In addition, Diana and co-workers use a pair of repeller electrodes to reflect back into the beam those positrons which are scattered to backward angles.

However, from the experimental parameters, such as magnetic-field strength, beam and chamber radii, it may be shown (see the Appendix) that there is a certain critical angle, which is a function of the impact velocity, for

which these measures will not confine the scattered positrons to the beam. Thus, a loss of flux of scattered positrons appears in the ionization, excitation, and elastic channels, introducing an underestimation of these processes. Consequently, an overestimation of the positronium formation cross section results, since it is deduced from a knowledge of these cross sections.

Since the two experiments differ in detail, we will discuss each individually. Also, we note that while the cross section for the sum of single charge transfer and transfer ionization (positronium formation) σ_{10}, is measured by one of the experiments, single capture alone is measured by the other. However, as the transfer-ionization cross section is expected to be very small (about two orders of magnitude smaller than single capture), we will use the notation σ_{10} to denote the cross sections measured in both experiments.

Fromme *et al.* determined the cross section for single charge transfer by observing the difference between the single ionization cross section and the cross section for production of He^+. The single-ionization cross section σ_{si} is deduced by counting in coincidence the detection of an outgoing positron and a He^+ ion, while the sum of single ionization and single charge transfer σ_{He^+} is found from the rate of He^+ detected. Thus, the single charge-transfer cross section is the difference $\sigma_{He^+}-\sigma_{si}$. In this case, we see that the experiment attributes to positronium formation of those positrons that are removed from the beam. However, positrons scattered to angles beyond the confinement angle after ionizing collisions will also be removed from the beam. This loss of positrons decreases the number of coincidences that determine σ_{si} and is therefore also attributed to positronium formation.

Of course, this loss of flux influences not only the measured single charge-transfer cross section but also the ionization cross section. We find that the loss of flux is always less than 20% of the ionization total cross section but is as large as ten times (at $v=4.47$ a.u.) the single charge-transfer cross section.

In order to demonstrate that this experiment measures a combination of the single charge-transfer cross section and some fraction f_{iB} of the ionization cross section, we have calculated the cross section for the loss of flux of positrons due to incomplete confinement and compared this quantity with the experimental values of Fromme *et al.* (The subscript "B" indicates here and below the result for the parameters of the experiments by Fromme *et al.* at Bielefeld.) This comparison is presented in Fig. 2(a). The quantity $f_{iB}\sigma_i$ is given by

$$f_{iB}\sigma_i = 2\pi \int_{\theta_c}^{\pi} \sin\theta \, d\theta \frac{d\sigma_i}{d\Omega} , \tag{17}$$

where θ_c is the confinement angle defined in the Appendix and the range of integration represents the range of angles for which confinement is not possible in the apparatus. As may be clearly seen from Fig. 2(a) the calculated total loss of positrons $\sigma_{10}+f_{iB}\sigma_i$ agrees well with the measured cross section at the higher velocities where the lack of confinement is significant.

At lower velocities the adjustment is negligible since

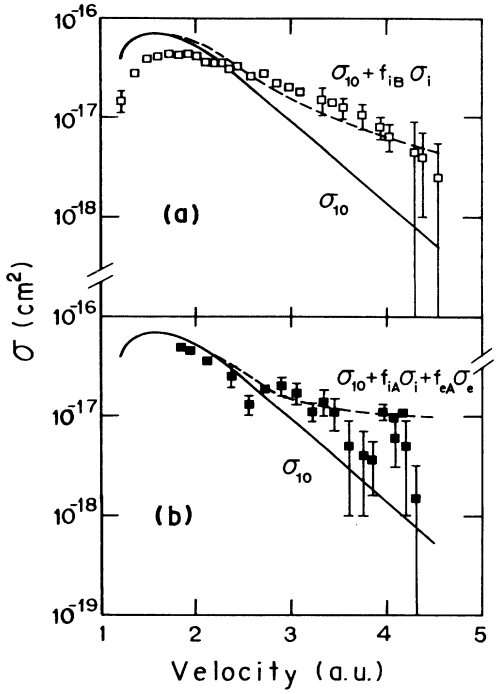

FIG. 2. The total cross section for charge transfer in positron-helium collisions. (a) Experimental measurements of Fromme *et al.* (Ref. 7) (open squares), CTMC2 (solid curve), and CTMC2 charge-transfer cross section plus the fraction not confined of the ionization cross section (dashed curve). (b) Experimental measurements of Diana *et al.* (Ref. 6) (solid squares), CTMC2 (solid curve), and CTMC2 charge-transfer cross section plus the fractions not confined of the ionization and elastic cross sections (dashed curve).

the wide-angle scattering constitutes only a tiny fraction of the total positronium formation cross section. The disagreement between our CTMC results and the experiment at velocities less than about 2 a.u. arises due to the fact that classically no threshold exists for capture and must be approximated as described in Sec. II. Thus in this velocity regime the CTMC model differs from the experiment which we believe is not seriously affected by the lack of confinement.

In the experiments of Diana and co-workers, the positronium formation cross section is estimated by observing the attenuation of the incident positron beam. As we have shown above, the cross section for the loss of flux can include a portion of the ionization cross section due to the lack of total confinement. In the experiment of Fromme *et al.* the beam attenuation is measured in coincidence with the production of He^+ ions and, therefore, loss of flux due to wide-angle scattering in elastic or excitation collisions is discriminated against. Here, however, since no coincidence measurement is made, these other channels in which lack of confinement might occur will also contribute to the measured loss of flux cross section.

Therefore, the contribution to the loss of flux cross section due to large-angle scattering in some channel α for this experiment is

$$f_{\alpha A}\sigma_\alpha = 2\pi \int_{\theta_{c\alpha}}^{\pi-\theta_{c\alpha}} \sin\theta \, d\theta \frac{d\sigma_\alpha}{d\Omega} , \quad (18)$$

where the range of integration, from θ_c to $\pi-\theta_c$ is chosen since the apparatus of Diana and co-workers includes repeller electrodes to deflect back into the beam the positrons scattered to angles greater than $\pi-\theta_c$. (The subscript "A" indicates the result for the parameters of the experiments by Diana and co-workers at Arlington.) The positrons scattered within the range θ_c to $\pi-\theta_c$ are lost from the beam due to collisions with the scattering chamber. The contribution to the loss of flux due to large-angle scattering in ionizing collisions has been evaluated using the present theoretical calculations. Similarly, the contribution from elastic scattering has been evaluated by numerical integration of the theoretical differential cross sections of Gupta and Mathur.[22] We have also found that the contribution due to wide-angle scattering in excitation is negligible (Madison and Winters[23]) in the velocity range of consideration.

Thus, we display in Fig. 2(b) the results of this experiment along with the estimated loss of flux cross section $\sigma_{10}+f_{iA}\sigma_i+f_{eA}\sigma_e$. As in the case of the experiment by Fromme *et al.*, this calculated loss of flux cross section agrees with the experimental data points which have the smallest quoted uncertainties. However, the data of Diana and co-workers also indicate that within these uncertainties, there should be some oscillations in the cross section. These oscillations were not observed by Fromme *et al.*, and, to our knowledge, are not predicted by any existing theoretical treatment.[3]

IV. RESULTS FOR KRYPTON

Recently, Diana *et al.*[8] have undertaken the measurement of the positronium formation cross section in positron-krypton collisions. Stimulated by these measurements and our findings of comparisons of single-electron removal processes in positron and proton impact of hydrogen and helium,[24] we have calculated ionization and charge-transfer total cross sections for these projectiles colliding with krypton. One of our goals has been to extend this early work in which we compare the positron and proton cross sections at equal impact velocities. Consideration of the many-electron target krypton allows us to test whether or not the effects we have found in simpler gaseous targets are also present and determine if any new effects arise. Another goal is to try to determine if the same discrepancy between our calculations and the experimental measurements exists, and if so, whether or not they can be explained in a similar manner.

Furthermore, by calculating proton-krypton cross sections we have been able to benchmark our models. For example, in Fig. 3 we present the total cross sections for both single ionization and free-electron production in the collision of protons with krypton. In this figure we display the results of our CTMCM*n* models where we have included either six electrons, representing the outer subshell of krypton (CTMCM6) and where we have included all subshells (CTMCM36). In the case of free-

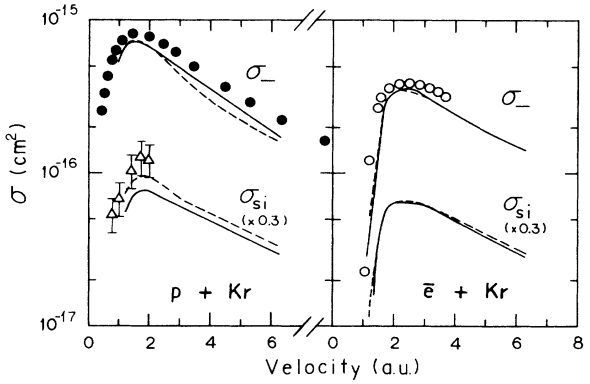

FIG. 3. The total cross sections for single ionization and for free-electron production in collisions of protons and positrons with krypton: experimental measurements of Rudd *et al.* (Ref. 25) (solid circles), experimental measurements of Dubois (Ref. 26) (open triangles), CTMCM36 (solid curves), CTMCM6 (dashed curves), and experimental measurements for electron-impact from Stephan *et al.* (Ref. 27) (open circles).

electron production, both models agree well with experiment at lower velocities. At higher velocities the model which includes all subshells yields a cross section which is about 20% higher than the model with only the outer subshell and is also in good agreement with experiment. We note that for single ionization, the CTMCM6 model agrees better with experiment than the CTMCM36 results, but this may well be accidental, since we believe that it overestimates the single-ionization cross section. The reason for this behavior is that it is less probable to remove only one electron in the CTMCM36 model than in the CTMCM6 model, which reflects the tendency for multiple ionization to dominate single ionization in many-electron atoms.

Also in this figure we present the total cross sections for single ionization and for free-electron production in positron-krypton collisions, as calculated using both the CTMCM6 and CTMCM36 models. For positron impact, we see that the differences between these two models are smaller than they are for proton impact. This reflects the fact that due to their small mass, positrons do not possess sufficient energy to remove an inner-shell electron from krypton at these intermediate collision velocities. Therefore, noting this agreement between these two models, we have calculated the ionization differential scattering cross sections which we will discuss later using the CTMCM6 model. For comparison, we also present in this figure experimental data for free-electron production in collisions of electrons with krypton. As has been already demonstrated for helium targets,[7,24] the ionization cross section for positrons is quite similar in magnitude to that of electrons in this velocity range. Figure 3 shows that a similar conclusion is obtained for krypton.

We note for completeness that the models that we have used do not contain any mechanism for final-state rearrangement. Specifically, if in the ionization process an electron is removed from an inner shell, Auger relaxation would result in the ejection of additional electrons. We

estimate that in the impact-velocity range considered here, inclusion of Auger events would not modify our single-ionization cross section by more than 15%. Regarding free-electron production, DuBois and Manson[28] have argued that below a velocity of approximately 3 a.u. the Auger contribution should be negligible. They further argue that above about $v=6$ a.u. Auger relaxation should dominate. Thus, we expect that in the velocity range considered here, inclusion of final-state rearrangement would increase the calculated free-electron production cross section at large velocities.

In Fig. 4 we present the results of our calculation of the total cross section for charge transfer in collisions of both protons and positrons with krypton. For proton-krypton collisions we have again used both the CTMCM6 and CTMCM36 models. As the figure indicates, at low velocities these models agree well with each other and with experimental measurements. However, as velocity is increased we note that capture from the inner shells of krypton begins to become significant and therefore the model which treats all the electrons yields a larger cross section. To illustrate this dependence we have also included in the figure a curve representing the M-shell contribution to the cross section. If this contribution is added to the cross section predicted by the CTMCM6 model, which includes only the outer shell, one sees that this accounts for most of the difference between CTMCM6 and CTMCM36 results. We have observed that our calculations agree well with the experimental data of Horsdal-Pedersen and Larsen[29] as to the relative importance of the M shell to the total cross section.

For both proton and positron impact of krypton at the higher velocities considered here, we expect that our CTMC treatments overestimate the charge-transfer cross sections due to the fact that capture may proceed to classically allowed states which are too tightly bound. This overestimation, which has been observed previously, does not affect the conclusions that we draw, however, since

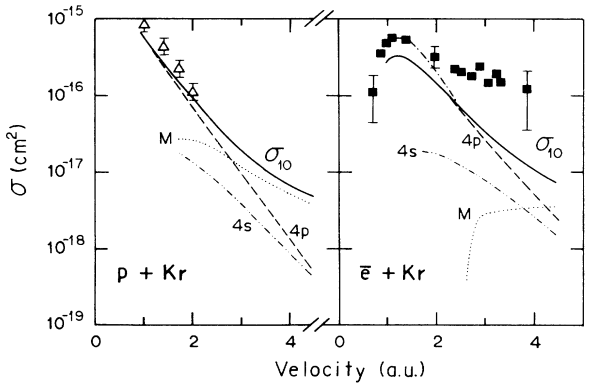

FIG. 4. The total cross section for charge transfer in collisions of proton and positrons with krypton: experimental measurements of DuBois (Ref. 26) (open triangles), experimental measurements of Diana *et al.* (Ref. 8) (solid squares), CTMCM36 (solid curves), CTMCM6 (dashed curves), 6 CTMCM (dot-dashed curve), and 4s and M-shell contributions from the CTMCM36 (dotted curves).

the integrated wide-angle ionization and elastic cross sections are much larger in magnitude than the charge-transfer cross sections.

For positron impact, this figure indicates that most of the difference between the CTMCM6 and CTMCM36 results may be attributed to the M-shell contribution. We note that in this velocity range, the M-shell cross section is generally much smaller for positrons than for protons due to the positron's much smaller mass and energy, but at the highest velocity considered here they become roughly equal. At still higher energies, it is expected that the cross section for positrons become larger than that for protons.

In Fig. 4 we also present the capture cross section computed using the 6CTMCM model in which six electrons are explicitly included. For proton impact, the 6CTMCM and the CTMCM6 models are found to agree, and therefore, we only present our calculations for incident positrons. As may be seen in the figure, the explicit inclusion of all six outer electrons significantly changes the total cross section at small impact velocities in comparison with the independent-electron approximation value. We find that a dynamical correlation between the electrons exists despite the absence of interaction between them. This correlation between electrons takes place through the coupling between the movement of the electrons and the positron. Further, the increase in the capture cross section is due to multiple-scattering events in which the positron first interacts with one or more of the six explicitly included electrons being deflected and/or accelerated into such a trajectory that it readily vector momentum matches with another of the electrons. For heavy-ion impact this coupling does not significantly affect the total cross section since the trajectory of the projectile is almost unaffected.

In our previous work we have calculated the ratio of the positron-ionization total cross section to that for protons, as well as the ratio for charge transfer. These ratios have been explained in terms of a model of the differences in the collision dynamics arising due to the differences in projectile mass. In the systems considered before[3,4,24] (i.e., hydrogen and helium), the velocity range of 1 to 4.5 a.u. was sufficient to allow us to draw some conclusions as the asymptotic behavior of the capture ratio. However, in krypton, since as velocity is increased the influence of the various subshells also increases in importance, this limited velocity range is no longer sufficient to indicate the large velocity behavior. In fact, the asymptotic behavior of this ratio should be given by the cross sections from the K shell. As different subshells begin to play an important role we also expect the ratio to display inflections. That is, the velocities for which each subshell becomes important for capture by protons or by positrons is different due to the mass difference between these two projectiles (see Fig. 4).

We may, however, conclude that positrons are more likely to capture an electron from krypton than equivelocity protons at high intermediate velocities. Specifically, at a velocity of 4.47 a.u. the positron charge-transfer cross section is about 1.5 times as large as the corresponding proton cross section. This ratio is much small-

er than in hydrogen or helium where the same shells contribute for both projectiles. If we consider only capture from the outer shell of krypton, the ratio is approximately nine, clearly illustrating that the ratio is very sensitive to the subshells accessible to the projectiles. In hydrogen and helium, the greater ability of positrons to vector momentum match with a target electron accounts for their enhanced capture cross section relative to protons, but in krypton, this ability is not as great an advantage. That is, even though the positron may readily vector momentum match, the proton may remove any one of a larger number of electrons.

As to the ratio for ionization, these calculations indicate that at high intermediate-collision velocities, positrons and protons are equally likely to singly ionize krypton. However, the free-electron production cross sections converge much more slowly as velocity is increased. For example, at $v=4.47$ a.u. the proton cross section is a factor of 1.4 greater than that for positrons. At smaller velocities, around the maximum of the cross sections, the proton cross section is about twice as large as the positron cross section. This enhancement for free-electron production by protons is due to the greater probability that protons will remove more than one electron from krypton. Equivelocity positrons, due to their smaller mass and therefore energy, are less likely to do so.

In Fig. 4 we also include the recent experimental determination of the charge-transfer cross section in positron-krypton collisions as measured by Diana and coworkers.[8] We see that, as in the case of positron-helium collisions, the slope and magnitude of the experimental cross sections at high intermediate velocities disagree with our calculations. Below we illustrate how this disagreement may be resolved in a manner similar to that which we have used for the measurements in helium. That is, by calculating the loss of flux of positrons due to the lack of confinement of positrons scattered to large angles after ionizing and elastic collisions.

To this purpose, we first display in Fig. 5 CTMCM6 calculations of the ionization differential cross section as a function of the scattering angle for krypton. This figure shows that conclusions similar to those for helium may be drawn as to the degree of wide-angle scattering at these relatively large velocities. Furthermore, at a velocity of 3.83 a.u. we include results of our 6CTMCM model which, we note, agree well with the independent-electron approximation results. We have also calculated total cross sections using this six active-electron model throughout the velocity range under consideration and find that, in contrast to the cross sections for capture, the ionization cross sections do not strongly depend on the differences between the CTMCM6 and 6CTMCM models.

To demonstrate that we may account for the difference between the measured cross section and our theoretical cross section we proceed as in Sec. III and compute the fraction of the positron flux which escapes confinement. From Eq. (18) we compute this fraction for ionization directly from our calculated differential cross sections. We have estimated the elastic cross section for positron impact from experimental measurements for electron impact[30] as, to our knowledge, no published measurements of the elastic differential scattering cross sections for positron-krypton collisions exist. Taking into consideration theoretical calculations by Nahar and Wadehra[31] of the elastic differential cross sections in collisions of positrons and electrons with argon, we expect that the magnitude of the elastic cross sections for electron or positron impact on krypton should not differ too much when integrated over the angular range of θ_c to $\pi-\theta_c$. In fact, performing this integration of the elastic differential cross section for electron and positron impact of argon of these authors we find that they differ by less than a factor of 2 for velocities greater than 2.7 a.u. Also, we expect that the differential cross section at large angles in the excitation channel should be at least one order of magnitude below the ionization and elastic differential cross sections.

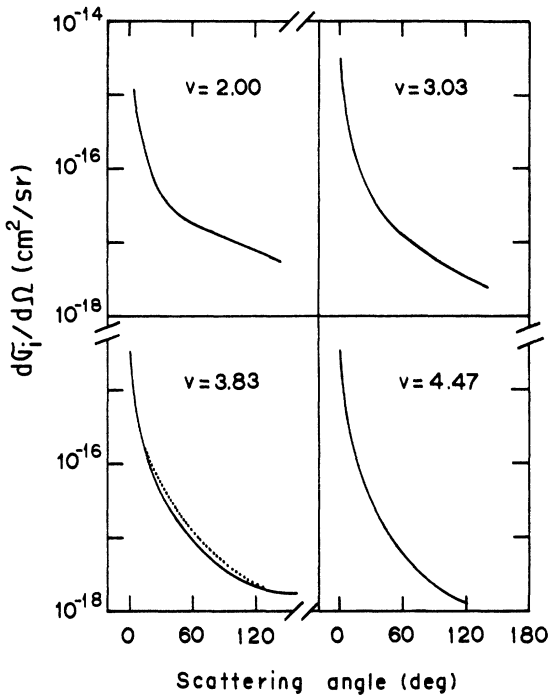

FIG. 5. The differential cross section as a function of the projectile scattering angle for ionization in collisions of positrons with krypton at several velocities as indicated: CTMCM6 (solid curves) and 6CTMCM (dotted curve).

Of course, the accuracy of the adjustments which we calculate is limited by the accuracy of each of these estimations of the true differential cross sections. Even though these adjustments do not represent absolute magnitudes they do, however, indicate the degree of enhancement of the measured cross sections over those which we believe on the basis of this model would be obtained with perfect large-angle scattering confinement.

Thus we demonstrate in Fig. 6 that the behavior of the experimental measurements can be reproduced by including the fractions of the ionization and elastic cross sections for those scattered positrons which escape confinement. That is, we plot $\sigma_{10}+f_{iA}\sigma_i+f_{eA}\sigma_e$ along with the experimental data of Diana *et al.*[8] and a fit of

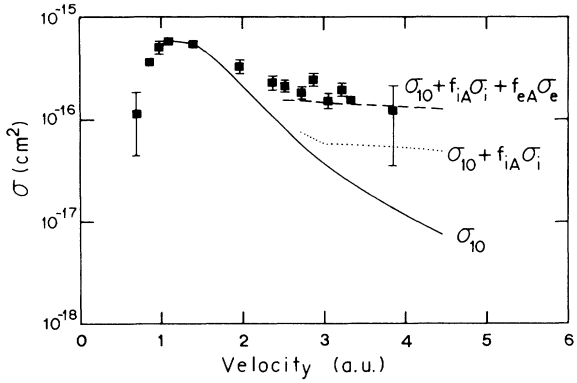

FIG. 6. The total cross section for charge transfer in positron-krypton collisions: experimental measurements of Diana *et al.* (Ref. 8) (solid squares), fit of the best CTMC calculations (solid curve), CTMC charge-transfer cross section plus the fraction not confined of the ionization cross section (dotted curve), and CTMC charge-transfer cross section plus the fractions not confined of the ionization and elastic cross sections (dashed curve).

our best CTMC calculations of the charge-transfer cross section. We have not performed calculations of $f_{eA}\sigma_e$ for impact velocities smaller than 2.5 a.u. since, according to Ref. 31, the total cross sections for positrons cannot be estimated in terms of those for electrons.

V. CONCLUSIONS

Using a variety of different CTMC models we have calculated the ionization differential scattering cross section for positron-helium and positron-krypton collisions. We have found that the cross section for the scattering of positrons to large angles in ionizing collisions is on the order of, or much greater than, the total cross section for positronium formation. Using these models we have also calculated the total cross section for single ionization, free-electron production, and charge transfer in positron- and proton-krypton collisions. Our results for protons are in generally good agreement with experimental measurements of these processes.

Our results have also indicated that in positron-helium collisions at high intermediate velocities, the explicit inclusion of two active electrons does not significantly influence the shape or magnitude of the calculated differential cross sections, nor does the use of a model potential, as compared to our independent-electron approximation, screened Coulomb interaction model. Similarly, for positron-krypton scattering, the differential cross section has been demonstrated to be relatively insensitive to the explicit inclusion of all six outer subshell electrons, an independent-electron model yielding reasonable results.

This insensitivity to the explicit inclusion of many active electrons is also present in the total cross sections for proton impact, due to the fact that the proton is nearly undeflected. However, for low-velocity collisions of positrons with krypton, the explicit treatment of the six outer electrons increases the total cross section for charge transfer due to a multiscattering mechanism in which one or more of the electrons first deflects the positron into such a trajectory that it may more easily vector momentum match with another electron. On the other hand, it is found that the explicit inclusion of the six outer electrons does not influence the positron-ionization total cross section.

Further, we find that the total cross sections for positron- and proton-impact ionization of krypton converge to the same value at high velocities for both single ionization and free-electron production. In the case of free-electron production, the convergence is slower as a function of velocity than for single ionization. This occurs since positrons, owing to their smaller mass, have less energy available for multiple ionization than do equivelocity protons. In the charge-transfer channel, we find that positrons are more likely to capture an electron from krypton than are protons at high velocity due to the positron's greater ability to vector momentum match with an orbital electron. The asymptotic value of the ratio of the positron to proton charge-transfer cross section is expected to generally increase but to experience inflections due to the changing importance of the various subshells of krypton.

Finally, we have demonstrated that by accounting for the loss of flux in the recent experiments measuring positronium formation due to positrons that are scattered to angles which allow them to escape confinement, the disagreement between theory and experiment may be resolved. We emphasize that even though the percentage of the ionization (or ionization plus elastic) cross section which is lost is very small, this contribution to the attenuation of the positron beam is equal to or larger than that due to positronium formation at high intermediate velocities.

ACKNOWLEDGMENTS

The authors would like to gratefully acknowledge the support of the Office of Fusion Research, U.S. Department of Energy.

APPENDIX: ESTIMATION OF THE EXPERIMENTAL CONFINEMENT ANGLES

Here we determine the angular scattering regions to which a positron may be deflected and still be confined to the beam in the experiments by Fromme *et al.*[7] and Diana and co-workers.[5,6,8] The reader is referred to the descriptions of the details of the individual experimental apparatuses given in the works of these groups. As the experimental techniques used by the two groups are different, we first analyze the confinement conditions in Ref. 7 and then those in Refs. 5, 6, and 8.

Fromme *et al.* have used an axial magnetic field to confine the positron beam to the forward direction as it passes through the target gas region. Let us now consider the motion of a positron after an ionizing collision with a target gas atom in this situation. In such an event the positron will be deflected to some laboratory angle θ referred to the incident beam, the z axis, with some final energy E_f. We decompose the final velocity of the posi-

tron into its parallel and perpendicular components relative to the z axis, and therefore to the B field,

$$v_{\parallel}=\sqrt{2E_f/m}\cos\theta\ , \tag{A1}$$

$$v_{\perp}=\sqrt{2E_f/m}\sin\theta\ , \tag{A2}$$

where m denotes the positron mass.

In the presence of the magnetic field, the subsequent motion of the positron will consist of a translation along the z axis with constant velocity $v_{\parallel}$ and a circular movement about the B field with a radius given by the well-known Larmor radius r_L

$$r_L=\frac{mv_{\perp}c}{|q|B}\ , \tag{A3}$$

where $|q|$ is the magnitude of the positron charge, c is the speed of light, and B is the magnetic-field strength.

In order that the positron be confined to the beam after such a collision, two conditions must be satisfied. First, the positron must not be deflected to backward angles, $\theta<90°$, and second, the radius r_L must be small enough so that the positron does not collide with the wall of the chamber. This second condition may be written as

$$r_L<\lambda(R_c-R_b)\ , \tag{A4}$$

where R_c is the radius of the scattering chamber and R_b the radius of the beam and where λ represents a geometrical factor relevant to the details of the experimental arrangement, or, making use of (A2) and (A3),

$$r_L=mc\sqrt{2E_f/m}\sin\theta/|q|B<\lambda(R_c-R_b)\ . \tag{A5}$$

Therefore, positrons will be irretrievably lost from the beam if the deflection angle is greater than 90° or greater than the angle given by solving (A5) for θ. Thus, the confinement condition is $\theta<\theta_c$, θ_c being the confinement angle defined as follows:

$$\theta_c=\begin{cases}90° & \text{for } K\geq E_f\\ \sin^{-1}[(K/E_f)^{1/2}] & \text{for } K<E_f\end{cases} \tag{A6}$$

where we define the term K as

$$K=\left[\frac{\lambda(R_c-R_b)|q|B}{\sqrt{2m}}\right]^2\ . \tag{A7}$$

The confinement angle is therefore determined by the experimental parameters R_c, R_b, and B. This form agrees with the estimate of the confinement angle given by Sinapius and Raith[32] which is

$$\theta_c=\begin{cases}90° & \text{for } E_0\leq 100\text{ eV}\\ \sin^{-1}\left[\left(\dfrac{79\text{ eV}}{E_0-E_i}\right)^{1/2}\right] & \text{for } E_0>100\text{ eV}\end{cases} \tag{A8}$$

where E_0 is the impact energy, E_i is the ionization potential of the target species, and the term E_0-E_i approximates the final energy of the positron. From (A8) we see that for the experiment of Fromme *et al.* the constant takes on the value of 79 eV. Thus we define $K_B=79$ eV. In Fig. 7 we display the behavior of this critical angle as a function of the incident velocity. The dotted curve indicates the result of applying the expression (A8).

In addition to the magnetic field used by Fromme *et al.* to confine the positrons to the beam, Diana and co-workers have utilized a set of electrodes in order to reflect back those positrons scattered into the backward direction. Therefore, the only confinement condition for these experiments is that the scattered positrons do not collide with the walls of the chamber; i.e., condition (A4). In other words, no restriction for the confinement is found when $K>E_f$. However, if $K<E_f$, those positrons scattered to angles in the range $\theta_c<\theta<\pi-\theta_c$ will be lost from the beam.

In order to estimate the confinement angle θ_c in the experiment of Diana and co-workers, we simply form the product $(R_c-R_b)B$ and compare it to the same quantity for the experiment of Fromme *et al.* From the articles by these two groups we find that R_c, R_b, and B are, respectively, 0.5 cm, 0.2 cm, and 300 G for the experiment of Fromme *et al.* and 1.0 cm, 0.25 cm, and 100 G for the experiment of Diana and co-workers, and the two products are then 75 and 70, respectively. Thus, we see that even though the magnetic fields differ by a factor of 3, this product of experimental parameters differs only by about 7%.

In Fig. 7 we also present the confinement angle for the experiment of Diana and co-workers (solid curve). The constant K for this experiment is found by multiplying the constant K_B by the ratio of the products obtained above and yields $K_A=73.7$ eV. As this figure indicates,

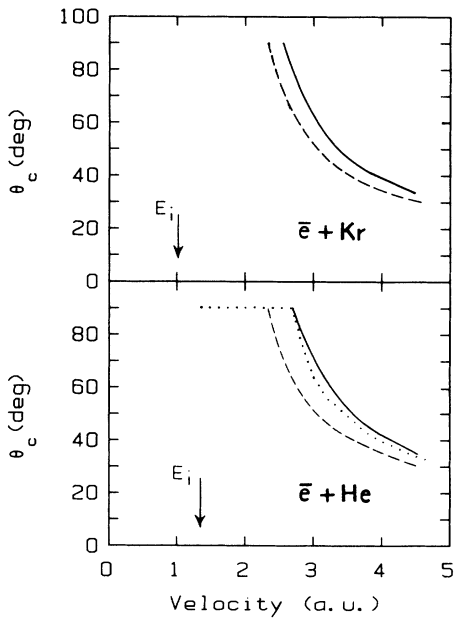

FIG. 7. The confinement angle as a function of positron impact velocity: confinement angle for the apparatus of Diana *et al.* in ionizing collisions (solid curves) and for elastic collisions (dashed curves) and confinement angle for the apparatus of Fromme *et al.* for ionizing collisions (dotted curve). E_i indicates the threshold energy for ionization of each target.

the confinement angle as a function of incident velocity is nearly the same in both the experiments.

Since Diana and co-workers have also performed measurements of the positronium formation cross section in positron-krypton collisions, we have also analyzed the confinement angle for this case. This angle can be obtained from expression (A6), using our CTMC calculation of the mean final positron energy as a function of incident velocity and the value deduced above for the constant K_A. The results of this calculation are displayed in Fig. 7 (solid curve).

As we indicate in the text above, loss of flux in positron-krypton measurements may also come from large-angle elastic scattering. Thus we also display in Fig. 7 the confinement angle for this channel (dashed curves). The critical angle can in this case be obtained by replacing the final energy in ionizing collisions [i.e., the denominator in expression (A8)], by the initial energy E_0.

[1]L. H. Andersen, P. Hvelplund, H. Knudsen, S. P. Moller, K. Elsenser, K.-G. Rensfelt, and E. Uggerhoj, Phys. Rev. Lett. **57**, 2147 (1986).

[2]N. C. Deb, J. H. McGuire, and N. C. Sil, Phys. Rev. A **36**, 1082 (1987).

[3]D. R. Schultz and R. E. Olson, Phys. Rev. A **38**, 1866 (1988).

[4]D. R. Schultz, C. O. Reinhold, and R. E. Olson, Nucl. Instrum. Methods **B42**, 527 (1989).

[5]L. S. Fornari, L. M. Diana, and P. G. Coleman, Phys. Rev. Lett. **51**, 2276 (1983).

[6]L. M. Diana, P. G. Coleman, D. L. Brooks, P. K. Pendleton, and D. M. Norman, Phys. Rev. A **34**, 2731 (1986).

[7]D. Fromme, G. Kruse, W. Raith, and G. Sinapius, Phys. Rev. Lett. **57**, 3031 (1986).

[8]L. M. Diana, P. G. Coleman, D. L. Brooks, R. L. Chaplin, R. M. Marroum, J. M. Alletto, J. K. Chu, J. P. Howell, M. S. Dababneh, and W. Liu, *Abstracts of Contributed Papers, Proceedings of the Fifteenth International Conference on the Physics of Electronic and Atomic Collisions, Brighton, 1987,* edited by J. Geddes, H. B. Gilbody, A. E. Kingston, and C. J. Latimer (Queen's University, Belfast, 1987).

[9]R. Abrines and I. C. Percival, Proc. Phys. Soc. **88**, 861 (1966).

[10]R. E. Olson and A. Salop, Phys. Rev. A **16**, 531 (1977).

[11]R. E. Olson, Phys. Rev. A **27**, 1871 (1983).

[12]R. Abrines, I. C. Percival, and N. A. Valentine, Proc. Phys. Soc. **89**, 515 (1966).

[13]R. E. Olson and T. J. Gay, Phys. Rev. Lett. **61**, 302 (1988).

[14]R. H. Garvey, C. H. Jackman, and A. E. S. Green, Phys. Rev. A **12**, 1144 (1975).

[15]C. Froese Fischer, *The Hartree-Fock Method for Atoms* (Wiley, New York, 1977).

[16]C. Moore, *Atomic Energy Levels,* Natl. Bur. Stand. (U.S.) Circ. No. 35 (US GPO, Washington, D.C. 1971).

[17]R. E. Olson, J. Ullrich, and H. Schmidt-Bocking, J. Phys. B **20**, L809 (1987).

[18]R. E. Olson, *Electronic and Atomic Collisions,* edited by H. B. Gilbody, W. R. Newell, F. H. Read, and A. C. H. Smith (Elsevier, Amsterdam, 1988), p. 271.

[19]C. O. Reinhold and C. A. Falcon, Phys. Rev. A **33**, 3859 (1986).

[20]J. H. McGuire and L. Weaver, Phys. Rev. A **16**, 41 (1977).

[21]J. M. Hansteen and O. P. Mosebekk, Phys. Rev. Lett. **29**, 1361 (1972).

[22]G. P. Gupta and K. C. Mathur, J. Phys. B **12**, 3071 (1979).

[23]D. H. Madison and K. H. Winters, J. Phys. B **16**, 4437 (1983).

[24]D. R. Schultz, Phys. Rev. A **40**, 2330 (1989).

[25]M. E. Rudd, R. D. DuBois, L. H. Toburen, C. A. Ratcliffe, and T. V. Goffe, Phys. Rev. A **28**, 3244 (1983).

[26]R. D. DuBois, Phys. Rev. Lett. **52**, 2348 (1984).

[27]K. Stephan, H. Helm, and T. D. Mark, J. Chem. Phys. **73**, 3763 (1980).

[28]R. D. DuBois and S. T. Manson, Phys. Rev. A **35**, 2007 (1987).

[29]E. Horsdal-Pedersen and L. Larsen, J. Phys. B **12**, 4085 (1979).

[30]J. F. Williams and A. Crowe, J. Phys. B **8**, 2233 (1975).

[31]S. N. Nahar and J. M. Wadehra, Phys. Rev. A **35**, 2051 (1987).

[32]G. Sinapius and W. Raith (private communication).